ENERGY
https://doi.org/10.1016/j.energy.2013.06.032

Development and comparative analysis of the modeling of an innovative finned-plate latent heat thermal energy storage system

Campos-Celador A.[a*], Diarce G.[b], González-Pino I.[c], Sala JM[c].

[a] ENEDI Research Group, Dpto. de Máquinas y Motores Térmicos, Escuela Universitaria de Eibar, University of the Basque Country UPV/EHU, Avda. Otaola 29, Eibar 20600, Spain.

[b] ENEDI Research Group, Dpto. de Ingeniería Minera, Metalúrgica y Ciencia de los Materiales, Escuela Universitaria de Ingeniería Técnica de Minas y Obras Públicas, University of the Basque Country UPV/EHU, Rafael Moreno Pitxitxi 2, Bilbao 48013, Spain.

[c] ENEDI Research Group, Dpto. de Máquinas y Motores Térmicos, Escuela Técnica Superior de Ingeniería de Bilbao, University of the Basque Country UPV/EHU, Alameda Urquijo s/n, Bilbao 48013, Spain.

[*] Corresponding author. Tel.: +34946017322. Fax: +34946017800. E-mail: alvaro.campos@ehu.es

ABSTRACT

This paper presents an innovative finned-plate latent heat thermal energy storage system for its integration in cogeneration systems. For optimization purposes it is very important to maximize the efficiency of the computational calculations. Therefore, three approaches are presented for the simulation of the same storage system: a numerical model, a simplified analytical one and a simplified numerical model.

These three models are applied to the simulation of a prototype which has been tested experimentally by means of a test benchmark for storage systems. The simplified analytical and simplified numerical models are implemented by the definition of an effective heat transfer coefficient. From the comparison of the results it was concluded that the three approaches gives rise to a good agreement with the test results. However, the simplified analytical model fails to predict long configurations. On the other hand, the simplified numerical model presents very good results for every configuration, reducing the computational cost of the numerical model from several hours to minutes.

Nomenclature

T	Temperature (ºC)
$\bar{T}$	Mean temperature (ºC)
c	Specific heat (J/kgK)
e	Width of the plates (m)

Greek symbol

λ	Thermal conductivity (W/mK)
ρ	Density (kg/m³)
μ	Dinamic viscosity (kg/ms)

Z	Height of the plate (m)
$\dot{m}$	Mass flow (kg/s)
M	Mass (kg)
x	X direction (m)
t	Time (s)
U	Heat transfer coefficcient (W/m^{2}K)
$\overline{U}$	Effective heat transfer coefficient (W/m^{2}K)
h	Sensible enthalpy (J/kgK)
H	Enthalpy (J/kgK)
f	Melting fraction
y	Y direction (m)
l	Length of the plate (m)
L	Phase change latent heat (J/kg)
Nu	Nusselt number
Ra	Rayleigh number
A	Heat transfer area (m^2)
y	Temperature efficiency
E	Stored energy (J)
s	Fin separation (m or cm)
w	Width of the channel (m)
Q	Heat transfer (W)

Abbreviations

$LHTES$	Latent Heat Thermal Energy Storage
TES	Thermal Energy Storage
PCM	Phase Change Material
NTU	Number of heat Transfer Units
HTF	Heat Transfer Fluid
N	Numerical approach
SN	Simplified numerical approach
AA	Approximated analytical approach
DSC	Differential Scanning Calorimmetry

Superscripts

l	Lower value
u	Upper value

Subscripts

c	Relative to the charging process
d	Relative to the discharging process
HTF	Relative to the HTF
e	Effective
PCM	Relative to the PCM
W	Relative to the plates and fins
pc	Relative to the phase change
P	Relative to the plate

1. INTRODUCTION

Thermal energy storage (TES) plays an important role in the rational use of energy, as it allows the decoupling between production and demand of thermal energy. In applications with intermittent energy generation, such as solar thermal systems or waste heat recovery, an appropriate TES system is essential. The thermal storage technology based on the use of phase change materials (PCMs) has recently raised an important practical interest. When using a PCM, energy transfer occurs when the material changes from solid to liquid, or liquid to solid. Unlike conventional (sensible) storage materials, PCMs absorb and release heat at a nearly constant temperature. They store from 5 to 14 times more heat per unit volume than sensible storage materials such as water, masonry, or rock [1]. These issues make them very interesting alternatives to conventional TES solutions, which commonly use water as storage medium, since they allow reducing the storage volume and improving the operating conditions of the whole system.

However, it should be considered that PCMs present some disadvantages over conventional TES systems. They generally present low thermal conductivities (between 0.2 and 0.7 W/m·K), which reduce the effective power in the charging and release of the thermal energy. Moreover, the specific price of these systems is significantly higher. Therefore, the designer plays a very important role based on the two main following considerations:

- It is necessary to adapt the power of the TES system to the requirements of the plant where it is integrated.
- It is necessary to find a geometry which allows reducing the complexity of the system and, consequently, its price.

Therefore, there is an implicit need for optimizing the design of different latent heat thermal energy storage (LHTES) configurations. Mathematical modeling is the best approach for applying any optimization method to the design of these systems, and a wide number of modeling approaches have been used for the simulation of LHTES systems of different nature [2]. Amongst all the possible LHTES configurations, in this paper, the modeling of an innovative finned-plate heat exchanger-based system for cogeneration is analyzed for optimization purposes.

The problem of predicting the behaviour of phase-change systems is difficult due to its inherent non-linear nature at moving interfaces. Owing to the complexity of the phase change problem very few analytical solutions are available in closed form. These are mainly for the one-dimensional cases of an infinite or semi-infinite region with simple initial and boundary conditions and constant thermal properties. Under these conditions, these exact solutions usually take the form of functions of the single variable $x/t^{1/2}$ and are known as similarity solutions [3,4]. A collection of similarity solutions and references is to be found in [5]. The specific characteristics of these solutions make them unsuitable for complex geometries and cases where the materials cannot be considered as homogeneous.

This deficiency is overcome by **numerical methods**. The main difficulty in the resolution of the phase-change problem is its inherent non-linear nature at moving interfaces, which is associated with the latent heat lost or absorbed at the boundary. Humphries and Griggs [6] studied numerically the phase change in a rectangular enclosure using straight fins as a heat

transfer enhancer in a 2-dimensional grid. The data were generated over a range of realistic sizes, material properties, and different kinds of thermal boundary conditions. Stritih et al. [7] handled heat transfer enhancement in the solidification process in a finned PCM storage with a heat exchanger both numerically and experimentally. Their conclusion was that the greatest influence on heat transfer was the distance between fins, being the thickness of the fins not so influential. Lamberg et al. [8] studied the numerical simulation of a finned rectangular slab for temperature control, using the enthalpy method and the effective capacity method. Numerical predictions were calculated with FEMLAB and compared to experimental data, showing good agreement between all the predictions. Analogously, a plenty amount of papers can be found in the bibliography dealing with the numerical simulation of PCM-based storage systems [9-11].

Moreover, Lamberg and Siren [12] presented a **simplified analytical model** which predicted the solid-liquid interface location and the temperature distribution of the fin in the solidification process with a constant end-wall temperature in the finned two-dimensional PCM storage. The analytical results were compared to numerical results. It was observed that the analytical model was more suitable to the prediction of the solid-liquid interface than to the temperature distribution in the PCM. Additionally more simplified analytical approaches can be found in the literature for PCM simulation [13].

Another simulation approach is the use of **simplified numerical models**. They offer, after taking some simplification on the mathematical modeling, a fast solution to the problem in comparison to the detailed numerical simulations, which commonly present high computational costs. Dolado et al. [14] set out different simulation models for a rectangular heat storage system without fins. A simplified 1D finite differences model was selected as the most appropriate model, offering a good compromise between accuracy and computational cost. Additionally, Hed and Bellander [15] developed a simulation model for the same application than Dolado but with just a single node for the PCM. Good agreement with the experimental results was obtained.

This paper presents three different modeling approaches for an innovative finned-plate LHTES system: (i) a numerical approach, (ii) a simplified analytical approach and (iii) a simplified numerical approach. The development of these models is presented and simulations are carried out for a given configuration, being compared with the experimental data obtained from the testing of a finned-plate LHTES prototype.

The paper is organised in seven different sections, as follows: Section 2 presents the innovative finned-plate LHTES system. In Section 3 the three proposed modelling approaches are developed. The LHTES prototype and the testing facility is presented in Section 4 and the 3 models are used to simulate the behaviour of the prototype, whose simulation results are presented and compared with the experimental data in Section 5. Finally, the results are discussed in Section 6 and the main contributions of the study are summarized in Section 7.

2. DESCRIPTION OF THE LHTES SYSTEM

Amongst all the possible combinations between shapes and heat enhancement techniques for LHTES systems, the compact finned flat plate configuration was chosen, which from now on will be referred to as finned plate technology. This technology presents the next advantages:

- It is based on compact flat plate heat exchangers, which is regarded as the most effective heat exchanger technology.
- The manufacturing process is simple, due to the fact that only straight surfaces are employed.
- By the definition of single plates, it presents high modularity.
- It presents a high surface to volume ratio, which allows getting significant storage and release powers.
- The whole LHTES system shows a rectangular shape, which makes its space integration easy.

The system is based on the definition of the single finned plate presented in Fig. 1 where the lid has been cut in order to show the inner finned structure.

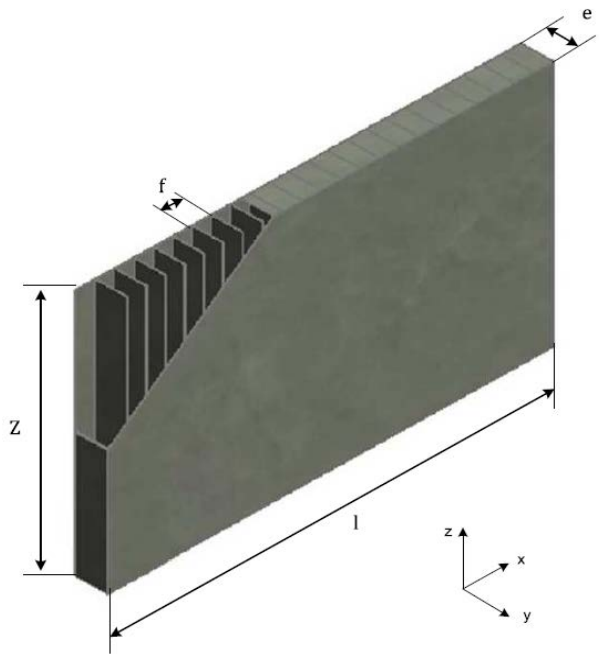

Fig. 1. 3D view of a single finned plate

The space between the fins within the plates is filled with PCM. RT60 paraffin from Rubitherm Gmbh was selected as PCM. Its phase change temperature is around 60ºC, which results very suitable for the application under analysis. A sample of this material was analyzed by means of a Mettler Toledo DSC1 differential scanning calorimeter. The obtained thermal properties are presented in Table 1 along with some physical properties given by the supplier, being the latter the density, the conductivity and the dynamic viscosity.

Table 1. Summary of the thermophysical properties of the PCM.

	T_{PC} (ºC)	λ (W/mK)	c (kJ/kgK)	ρ (kg/m^3)	L (J/kg)	μ (kg/ms)
RT60	53 (lower) 61 (upper)	0.02	2660 (solid) 2340 (liquid)	880 (solid) 770 (liquid)	123,506	3.705 x 10^{-5}

The phase change does not take place at a single temperature but through a temperature range. This is owed to the fact that the PCM is not homogeneous and contains additives which distort the phase change. The structure of the system (plates and fins) can be made by any metallic common material, such as stainless steel or aluminum, due to its high conductivity. For the present study, aluminum was chosen.

These plates are the modules that make up the whole system. They can be arranged in series or in parallel, giving rise to different LHTES system configurations that the designer should define in detail. In Fig.2 it can be seen an example in 2D consisting of 12 plates, arranged 6 in parallel and 2 in series. The heat transfer fluid, water in this case, flows through the channels formed between the plates.

Fig 2. 2D view of the LHTES of 12 finned plates

3. MODELING OF THE LHTES SYSTEM

The channels where the water flows through are very thin (in the order of few millimeters), as imposed by the compact heat exchanger technology in which the solution is based, and they are modeled in 1D in the direction of the flow as presented by Eq. 1. By means of a hydraulic study, it was observed that the turbulent regime would increase significantly the pressure drop of the system. For this reason, only laminar regime is considered for the flow.

$$\rho_{HTF}\, c_{HTF}\, w\, Z\, \frac{\partial T_{HTF}}{\partial t} + \dot{m}\, c_{HTF}\, \frac{\partial T_{HTF}}{\partial x} = -2\, U\, Z\, (T_{HTF} - T) \qquad \text{(Eq. 1)}$$

Here, the different modeling approaches are based on how the finned plates are discretized:

- When the plate is discretized in 2 dimensions (x and y) it gives rise to the numerical model (N). For this case, T would represent the temperature at the surface of the plate and U is the convection heat transfer coefficient.
- When the plate is discretized in a single node, it gives rise to the simplified analytical model (SA). For this case, T would denote the average temperature of the plate ($\bar{T}_p$) and U is the effective heat transfer coefficient, U_e.
- Finally, when the plate is discretized in 1 dimension (x), it gives rise to the simplified numerical model (SN). For this case, T would correspond to the average transversal

temperature of the surface of the plate ($\bar{T}_p$) and U is the effective convection heat transfer coefficient, U_e.

These 3 approaches are developed in detail in the next subsections.

3.1.Numerical model

The numerical model consists of solving the temperature field of the plates following the discretization presented in Fig 3. The discretization is made in the x and y direction and the heat transfer interaction between the HTF and the plates is presented.

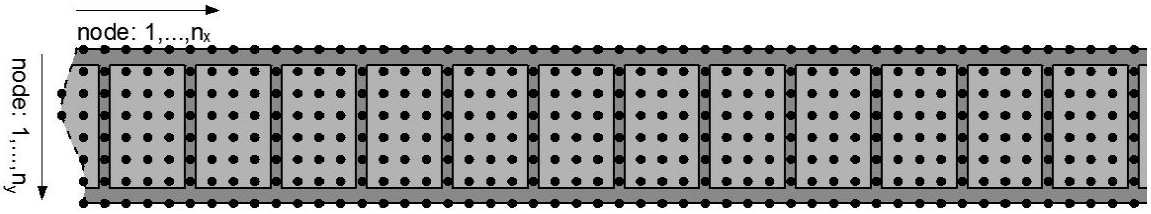

Fig 3. Discretization of a single plate by the numerical model

According to that discretization, the energy balance equations for the plates and fins and for the PCM are respectively:

$$\rho_W c_W \frac{\partial T_W}{\partial t} = \frac{\partial}{\partial x}\left(\lambda_W \frac{\partial T_W}{\partial x}\right) + \frac{\partial}{\partial y}\left(\lambda_W \frac{\partial T_W}{\partial y}\right) \quad \text{(Eq. 2)}$$

$$\rho_{PCM} \frac{\partial h}{\partial t} + \rho_{PCM} L \frac{\partial f}{\partial t} = \frac{\partial}{\partial x}\left(\frac{\lambda_e}{c_{PCM}} \frac{\partial h}{\partial x}\right) + \frac{\partial}{\partial y}\left(\frac{\lambda_e}{c_{PCM}} \frac{\partial h}{\partial y}\right) \quad \text{(Eq. 3)}$$

where f represents the fraction of melted material. The resolution of the PCM's temperature field is made by applying the enthalpy method [16], which relates the enthalpy of the PCM with its temperature. The enthalpy is the summation of the sensible and latent terms as follows:

$$H = h + f\,L \quad \text{(Eq. 4)}$$

The relationship between enthalpy and temperature is provided from the DSC analysis carried out for the characterization of the PCM, and through which, the value of f can be obtained, considering that:

$$f = \begin{cases} 0 & H \leq c_{PCM,s}\, T_{pc}^{l} \\ f & c_{PCM,s}\, T_{pc}^{l} < H < c_{PCM,l}\, T_{pc}^{u} + L \\ 1 & H \geq c_{PCM,l}\, T_{pc}^{u} + L \end{cases} \quad \text{(Eq. 5)}$$

The conductivity of the PCM is treated as an effective thermal conductivity term, as shown by Eq. 6. The effect of the natural convection in the melting is treated implicitly. The correlation for the effective conductivity for this kind of LHTES system was determined by the author in a recent paper as function of the Rayleigh number [17], and it is presented in Eq. 7.

$$\lambda_{eff} = \lambda_{PCM}\, Nu \qquad \text{(Eq. 6)}$$

$$Nu = 0.345\, Ra^{1/4} \qquad \text{(Eq. 7)}$$

On the other hand, the heat transfer between the HTF and the surface of the plates is governed by forced convection under laminar regime, for which a constant value of Nu equal to 8.235 for the constant heat flow assumption is considered [18].

3.2.Simplified analytical model

The simplified analytical model consists of solving the temperature field at the plates following the discretization presented in Fig. 4 for the half plate and half channel. In this case, the whole system is discretized as a single node.

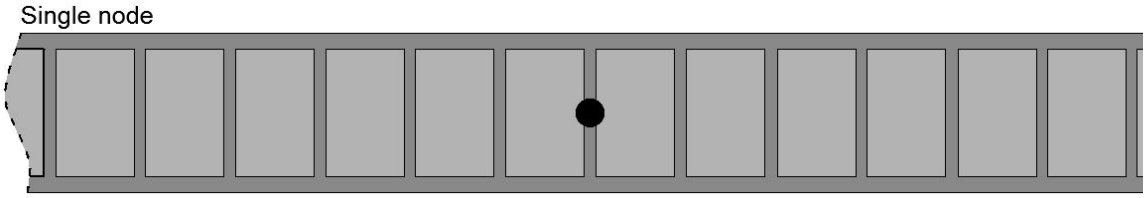

Fig. 4. Discretization of a single plate by the simplified analytical model

The simplified analytical model is based on the work made by Bejan [19] on sensible storage. After including some modifications, that work was extended for simulation of LHTES systems. The isothermal condition is introduced to the plates considering that the whole LHTES system presents the same temperature, being initially at T_0. In our case, the system is assumed to be uniformly at T_p at any instant. The phase change can be modeled considering that the effective specific heat of the PCM varies with its temperature and that is related with the variation of the enthalpy during the phase change obtained from the DSC analysis ($c_{PCM} = \partial H/\partial T$). Neglecting the storage capacity of the water and writing the energy balance for an incremental length dx, we have:

$$\dot{m}\, c_{HTF}\, dT_{HTF} = -U_e\, A\, dx(T_{HTF} - T_p) \qquad \text{(Eq. 8)}$$

where A represents a local heat transfer area per length unit (commonly referred to as wetted perimeter) and U_e is the effective heat transfer coefficient between HTF and PCM based on A.

Integrating over the overall length of the channel, from $x = 0\ (T_{HTF} = T_{in})$ to $x = l\ (T_{HTF} = T_{out})$ the next expression is obtained:

$$\frac{T_{out}(t) - T_p(t)}{T_{in} - T_p(t)} = \exp\ (-NTU) \qquad \text{(Eq. 9)}$$

where $NTU = U_e\ A/(\dot{m}\ c_{HTF})$ is the Number of Transfer Units. Defining the temperature efficiency as $y = 1 - \exp\ (-NTU)$, the previous expression can be rewritten as:

$$T_{out}(t) = T_{in} \exp\ (-NTU) + y\ T_p(t) \qquad \text{(Eq. 10)}$$

Setting out the energy balance in the storage media and considering Eq. 8, a general solution for T_p can be obtained:

$$M_{PCM} \int_{T_0}^{T_P} \frac{c_e\ dT_p}{y\ (T_{in} - T_p(t))} = \dot{m}\ c_{HTF}\ t \qquad \text{(Eq. 11)}$$

where both T_p and T_{out} approach T_{in}, and are functions of time. c_e is defined as the effective heat capacity of the plates. This term includes the storage capacity of the PCM as well as that of the walls and fins. Considering that the value of c_e varies with the state of the PCM and, therefore, with its temperature, it must be defined by parts. Analogously, an effective value of y (y_e) would be obtained.

Integrating over the time from $t = 0\ (T_{PCM} = T_0)$ to t, a general expression for the PCM temperature during the charging process can be obtained.

$$T_p(t) = \begin{cases} T_{in} - (T_{in} - T_0) \exp(-y\ \gamma_{e,s}\ t) & T_p < T_{pc}^{l} \\ T_{in} - \dfrac{(T_{in} - T_0)^{\frac{c_{e,s}}{c_{e,m}}}}{(T_{in} - T_{pc}^{l})^{\left(\frac{c_{e,s}}{c_{e,m}} - 1\right)}} \exp(-y\ \gamma_{e,m}\ t) & T_{pc}^{l} \le T_p \le T_{pc}^{u} \\ T_{in} - \dfrac{(T_{in} - T_0)^{\frac{c_{e,s}}{c_{e,l}}}}{(T_{in} - T_{pc}^{l})^{\left(\frac{c_{e,s}}{c_{e,l}} - \frac{c_{e,m}}{c_{e,l}}\right)} (T_{in} - T_{pc}^{u})^{\left(\frac{c_{e,m}}{c_{e,l}} - 1\right)}} \exp(-y\ \gamma_{e,l}\ t) & T_p > T_{pc}^{u} \end{cases} \qquad \text{(Eq. 12)}$$

An analogous expression is obtained for the solidification/discharging. It must be taken into account that this model does not consider the heat exchange of the HTF with the surface of the plate, but with the whole section of the plate represented by the value T_p. A single heat transfer coefficient (U_e) is defined, which lumps the heat convection and the transient effects

during the charging and discharging. The detailed definition and calculation of this term is covered in the Appendix.

3.3.Simplified numerical model

The simplified numerical model consists of solving the temperature field of the plates following the discretization presented in Fig. 5, where the whole system is only discretized in the X axis.

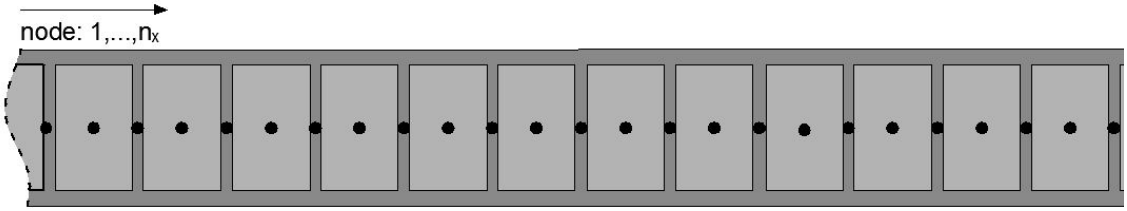

Fig. 5. Discretization of a single plate by the simplified numerical model

This is set out mathematically as follows:

$$\rho_e \, c_e \, e \frac{\partial T_p}{\partial t} = 2 \, U_e \, (T_{HTF} - T_p) \qquad \text{(Eq. 13)}$$

Where the subscript e means the effective magnitude of the plate obtained from the configuration of each node-cell. In the case of the specific heat, c_e, it also contains the effect of the phase change derived from the enthalpy-temperature curve given by the DSC.

This is an intermediate solution between the previously presented two models. Here, the temperature field of the plate section is represented by a single value, that varies along the x direction. In this case, it is also necessary to include a lumped U_e value, which is the same that was introduced in Section 3.2.

4. LHTES prototype and experimental facility

For the validation of the presented models, an experimental facility which is part of the facilities of the Laboratory for the Quality Control in Buildings (LCCE) of the Basque Government was employed. It is suitable for the testing of TES prototypes of different nature. A finned-plate LHTES prototype has been designed and constructed for validation purposes.

The experimental facility consists of two loops: one for the charging of the system and one for the discharging. It allows carrying out independent charging and discharging tests, as well as combined ones. The installation presents a set of elecromechanical valves that allows both controlling temperature levels and adjusting instantaneous flow rates, therefore, inlet conditions for the different tests can be controlled. The scheme of the installation is presented in Fig. 6, and its main characteristics are in Table 2.

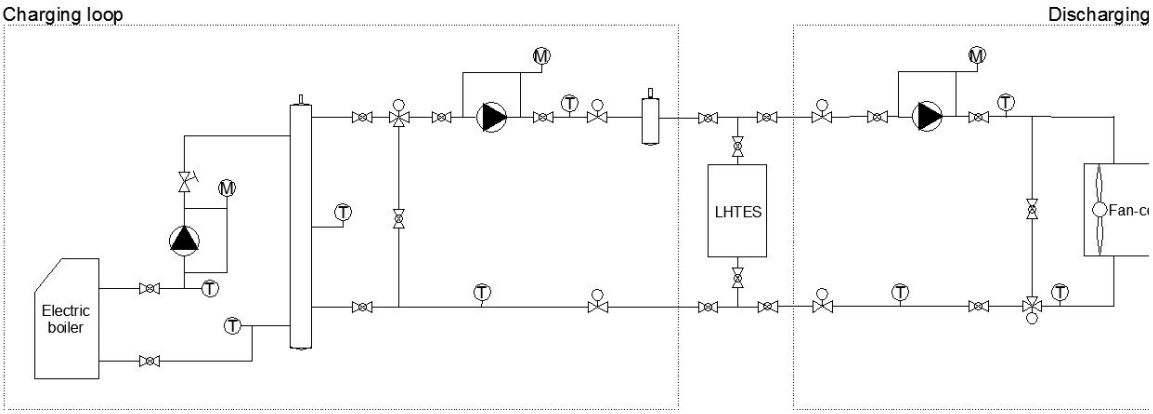

Fig. 6. Schematic view of the experimental facility

The analysis of the exchanged thermal power is based on the measurement of the temperature difference between the inlet and the outlet, and the mass-flow flowing through the prototype as described by Eq. 14, where c_{HTF} is evaluated for the average temperature of the water flowing through the system.

$$Q_i = \dot{m}_i \, c_{HTF} \, (\Delta T)_i \qquad \text{(Eq. 14)}$$

For the measurement of the mass flow, an electromagnetic flow meter is used, with an accuracy better than ±0.25% for a measurement range that varies between 0.2 and 10 m/s. On the other hand, two 2-wire Pt500 thermoresistance sensors are placed in the inlet and the outlet of the prototype. The measurements of these sensors were calibrated by intercomparation with a reference standard (calibrated by the Northern Temperature Primary Laboratory) in a thermostatic bath (±0.02ºC). Then, considering the accuracy of the sensor, reference standard and acquisition system, the accuracy of the sensors has been estimated to be below ±0.15ºC.

The propagation of uncertainties in the thermal power measurement was analyzed following specifications of [20]. Thus, following these guidelines, the uncertainty of the stored or released thermal power is determined to be of ±0.49% of the experimentally measured thermal power.

Table 2. Summary of the main characteristics of the experimental facility

Heat production power	10.5 kW
Heat release power	24.0 kW
Flow rate range ($\dot{m}$)	1.2 - 32 l/min
Working temperature range	20 - 90 ºC

As stated before, a finned plate LHTES system prototype was designed and constructed for validation purposes. It reproduces the behavior of a single channel-two plates LHTES system which exchanges heat with two halved finned plates and which is depicted in a red square in

Fig. 2. Two manifolds were placed at the inlet and the outlet of the prototype to assure a good HTF distribution. A view of the LHTES prototype is presented in Fig. 7 and its main characteristics are summarized in Table 3. The halved finned plates were manufactured in aluminum and the enclosure in methacrylate to allow visual inspection.

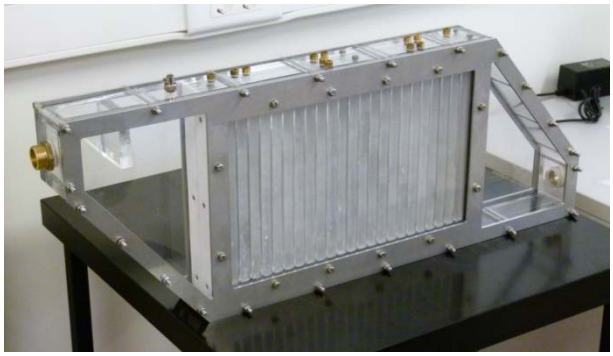

Fig. 7. Finned plate LHTES prototype

The thickness of both the walls and fins was fixed at 1.5 mm, which is the minimum value to ensure a good mechanical stability.

Table 3. Summary of the main characteristics of the finned plate LHTES prototype

Height of the plates ($\mathbb{Z}$)	0.2 m
Length of the plates/channel (ℓ)	0.345 m
Width of the plates (w)	0.049 m
Width of the channel (e)	0.002 m

It should be noticed that, since the finned plate LHTES prototype allows being opened, it makes it possible to test different PCMs and, therefore, further research with this LHTES solution.

Five charging-discharging cycles have been carried out. While the 4 first tests were used to prove the stability of the charging-discharging procedure, only the last one was considered for validation. The tests are carried out working between two temperature levels, 50 and 65ºC, which were selected as appropriated for domestic cogeneration. Thus, the charging process starts when the temperature of the system is steady at 50ºC and then a fixed value of 65ºC is imposed as a constant input. Similarly, the discharging process starts at steady 65ºC and a 50ºC setpoint is applied to the input. For both cases a flow rate of 0.04 kg/s was chosen, which ensures a laminar flow regime.

5. SIMULATIONS AND RESULTS

In this Section the results of the simulations are presented and compared with those obtained from the experimental tests. For the simulations, an AMD Turion Dual Core-Mobile 2.30 GHz with 6,00 GB RAM PC has been used.

The time and spatial discretization was previously optimized for the simulations, to reduce the simulation time without implying a decrease of the accuracy. Based on the results obtained, 1 second was selected as a time basis for all the simulations. The Numerical (N) simulations were carried out selecting a grid of 0.3 mm in the x direction and 1 mm in the y direction. On the other hand, the Simplified Numerical simulations were carried out selecting a node separation of 2 cm in the x direction. This value is sensibly larger than that in the N case, since the lumped nature of the discretization allows a larger grid size, as the geometric structure is implicitly included by the definition of the U_B value.

The results of both the simulations and the experimental tests for the charging process are presented in Fig. 8. For the sake of clarity, the results of the simulations are plotted every 2 minutes.

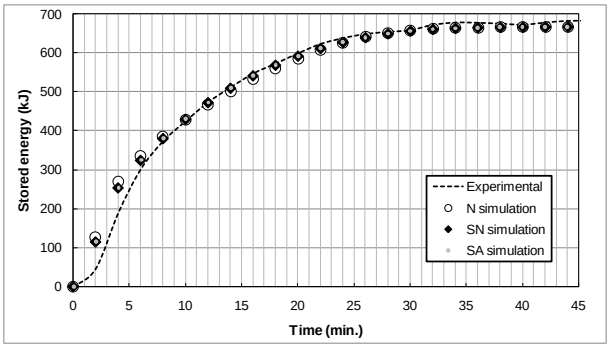

Fig. 8. Evolution of the stored energy during the charging process

As it can be observed, the three approaches agree very good with the experimental tests. It can be appreciated as well, that the whole charging process takes approximately 30 minutes to be completely finished. In the first five minutes of the simulations the stored energy is slightly higher than in the experimental test. This is caused by the effect of the heat stored in the inlet and outlet manifolds as it can be seen in Fig. 8. However, in real size finned-plate LHTES systems, the storage effect in these manifolds is negligible when compared with the storage capacity of the whole system.

The results of the simulations and the experimental test are presented in Fig. 9 for the discharging process.

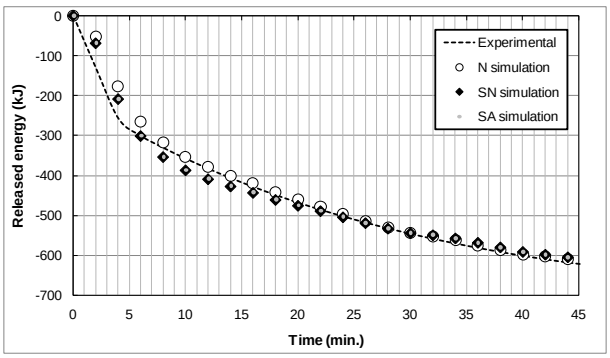

Fig. 9. Evolution of the stored energy during the discharging process

In this case, the results of the three simulation approaches show again a good agreement with the experiment. This time, the discharging process takes in the order of 45 minutes to be completed, sensibly more than in the charging, since the effect of the natural convection of the liquid phase is negligible during the solidification. Here again, a slight difference is found between the simulations and the experimental measurements during the first 5 minutes, which is also owed to the effect of the inlet and outlet manifolds.

Thereby, it has been observed that the three simulation approaches and the experimental tests offer very similar results for both the charging and discharging processes. These results and other associated implications are discussed in detail in Section 6 in order to obtain general conclusions of the numerical analysis.

6. DISCUSSION

As seen in Section 5, the three approaches agree fairly good with the experimental tests. The small discrepancy noticed at the beginning of the processes is due to the nature of the prototype, and would be negligible in full scale LHTES systems. However, the validity of these approaches for longer systems should be determined. Especially for the simplified analytical approach, where only a single node is used for modeling the whole plate.

For this purpose, a detailed study on the validity of the isothermal assumption was numerically performed. There, the predictions of the simplified analytical and the simplified numerical code for five lengths of the LHTES system (from 1 to 5 meters) were compared. For this analysis, the numerical simulation approach was not considered, owing to the good agreement shown with the simplified numerical approach, and to the high computational cost of the former, which would increase enormously the cost of this evaluation. The evolution of the stored energy for the five LHTES systems of different length during the charging process is illustrated by Fig. 10. The results are presented in a dimensionless form in order to facilitate the comparison between the different configurations.

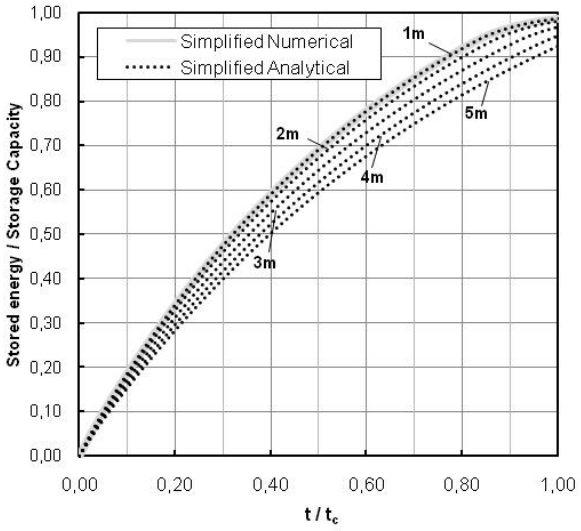

Fig. 10. Relation between the accuracy of the predictions of the simplified analytical approach with the length of the plate

As it can be observed, discrepancies between the two approaches begin to be noticeable for configurations larger than 2 meters. Therefore, it can be stated that the isothermal assumption of the plates is only valid for LHTES configurations below 2 meters, being that the range where the simplified analytical approach can be used confidently under the current operating conditions for the presented prototype.

The optimization of the design of this new kind of LHTES systems is amongst the objectives of the simulations presented in this paper. Thus, the computational time or CPU time plays an essential role in the evaluation of each approach, since optimization methods require a large number of simulations. In order to assess this aspect, a large enough LHTES system of 10 meters, which can represent a full scale prototype, was evaluated by the three simulation approaches. The required CPU times are presented in Table 4. The time for the discharging is slightly higher since the discharging process itself requires more time to get finished as it was reasoned in Section 5.

Table 4. CPU times required by the simulations of the 10 meters LHTES system

Simulation approach	CPU time for the charging	CPU time for the discharging
Numerical (N)	27.8 hours	34.2 hours
Simplified numerical (SN)	6 seconds	9 seconds
Simplified analytical (SA)	Negligible	Negligible

This way, it is found how the simplified approach presents a huge reduction of the CPU time. Fig. 11 shows the evolution of the stored energy during the charging given by both approaches normalized on a dimensionless basis. There, it can be appreciated that the results present again a very good agreement, even better than that obtained for the simulations of the prototype. This is caused by the fact that, now, as the length of the system has increased, the influence of the discretization in the flow direction is higher than that in the transversal direction. This allows reducing the cost the CPU time with a negligible difference in relation with the results of the Numerical simulation.

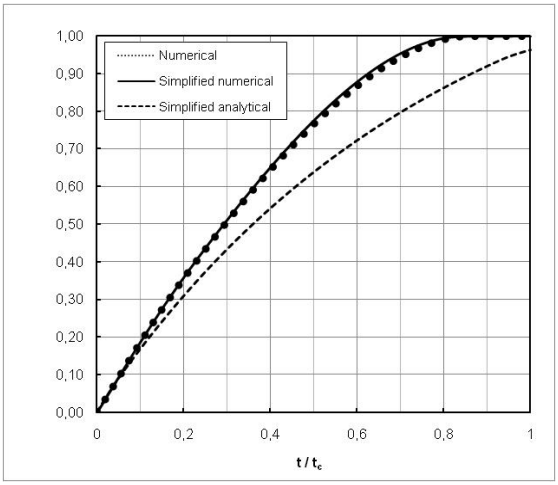

Fig. 11. Evolution of the stored energy during the charging process for the simulation of the 10 meters prototype

Hence, some general conclusions can be extracted from the analysis of the three simulation approaches. Amongst the three models, the numerical model is the most accurate, but it requires a big amount of computational time which makes it unfeasible for optimization processes where a large number of configurations might be evaluated.

The simplified numerical model is a versatile tool that can be used for every kind of finned-plate LHTES configuration. It is flexible enough to be integrated in dynamic simulations of whole plants where the inlet conditions vary with time, although some errors can be introduced when the charging or discharging processes are not finished. This is caused by the fact that the state of the plates is represented by a single temperature, neglecting the real temperature field. This fact is avoided when the numerical model is employed, as it considers the real distribution of temperatures within the plates.

The simplified analytical code is a useful tool for predesign purposes, when quick solutions are required. The operating conditions should remain constant and it is therefore not valid for the implementation in general-purpose simulation environments. The use of this model is subjected to the length of the LHTES system, which should not be forgotten when it is used.

For both the simplified analytical and simplified numerical codes, the U_e value must be determined. These values were obtained by the expression determined in the Appendix. However, they are exclusively valid for the selected PCM and encapsulation materials. This process should be updated when other materials are used both as storage medium or as encapsulation.

7. CONCLUSIONS

Three mathematical models suitable for the thermal modeling of LHTES systems, which are applied to an innovative finned plate system, have been developed: numerical (N), simplified analytical (SA) and simplified numerical (SN) models. These three models have different features which make them suitable for different purposes. Amongst them, the simplified numerical (SN) model is chosen as the most suitable for design and optimization purposes, and for its integration in general-purpose simulation software. Nonetheless the other two models, (N and SA) can complement the simulation capabilities for specific design purposes of the proposed LHTES solution.

ACKNOWLEDGEMENTS

The authors want to acknowledge the Spanish's Ministry of Economy and Competitiveness for the financial support through the project microTES (ENE2012-38633). Many thanks also to the Laboratory for the Quality Control in Buildings (LCCE) of the Basque Government.

Gonzalo Diarce and Iker González-Pino acknowledge the financial support of the Basque Government, through the Department of Education, Universities and Research's Personnel Research Training Program. Finally, the authors acknowledge DIKOIN for their technical support in the design and construction of the prototype, especially Alberto Cuadrado for his commitment.

APPENDIX

In this appendix the calculation of the effective heat transfer coefficient, U_e, used in the simplified analytical (SA) and simplified numerical (SN) approaches is covered in detail. The heat transfer coefficient U at any instant may be defined as follows:

$$U = \frac{Q}{A\,(T_{HTF} - \bar{T}_p)} \qquad \text{(Eq. A-1)}$$

This term embraces the forced convection between the HTF and the surface of the plate and the heat transfer within the plates and the PCM. Its value varies over the melting and solidification processes, being different for each process. However, our assumption lies in defining a constant effective heat transfer coefficient (U_e) for each one of these processes, $U_{e,c}$ and $U_{e,d}$ respectively. In order to define these new terms, it is imposed that the melting and solidification times are equal, using an instantaneous heat transfer coefficient or an effective heat transfer coefficient. This fact gives rise to the next two equations:

$$U_{e,c} = \frac{0.98\,E}{A\int_0^{t_c}(T_{HTF} - \bar{T}_p)\,dt} \qquad \text{(Eq. A-2)}$$

$$\bar{U}_{e,d} = \frac{0.98\,E}{A\int_0^{t_d}(\bar{T}_p - T_{HTF})\,dt} \qquad \text{(Eq. A-3)}$$

The melting and solidification are assumed to have finished when the stored or released thermal energy accounts for the 98% of the overall, defining so the melting and solidification times, t_c and t_d, respectively.

Noticing that the same values of $U_{e,c}$ and $U_{e,d}$ are valid for the simplified analytical and simplified numerical models, and considering the analytical expression for $\bar{T}_p$ given by the simplified analytical approach, the solution of these equations can be set out. However $\bar{T}_p$ also depends on U_e, and the equations to be solved are non-linear. This is overcome by applying the fixed point method. As initial guesses for the iterations, the time average values of U obtained from the numerical simulations are considered as follows:

$$(U_{e,c})_0 = \frac{\sum_0^{t_c} U_c}{t_c} \qquad \text{(Eq. A-4)}$$

$$(U_{e,d})_0 = \frac{\sum_0^{t_d} U_d}{t_d} \qquad \text{(Eq. A-5)}$$

This way, the solution of $U_{e,c}$ and $U_{e,d}$ uses the numerical simulations, first considering the time average values of U as initial values for the calculation of U_e and then by the iterative resolution of Eq.2 and Eq.3, where the melting and solidification time values are included. Due to the nature of the plates, it is not necessary to simulate the whole plates but single control cells, with a significantly lower computational cost. However, to perform a numerical simulation prior to each evaluation by the simplified analytical and the simplified numerical codes would not be operative and other solution is necessary.

An statistics-based method for the calculation of $U_{e,c}$ and $U_{e,d}$ is designed which is based on simulations of the numerical model. The same operating conditions defined in the main text are used here. The forced convection coefficient is that correspondent to laminar flow and 2 mm width channel (w), 1212.6 W/m^{2}K.

Among the different geometric variables of the plates, $U_{e,c}$ and $U_{e,d}$depend exclusively on the dimensions of the control macro-volume which, neglecting the height, are the distance between fins s and the thickness of plate e. In order to analyse this dependency, a large enough set of control macro-volumes is defined by combination of e and s values.

These variables are bounded considering big enough intervals to include all the designs that can result of interest for our application. Values of e between 1 and 5 cm are selected. Considering that the fin thickness is 1.5 mm, the minimum value of s is set at 1.15 cm, which corresponds to 1 cm between fin walls. The maximum value is set assuming that it should be a s value above which the effect of the fins is negligible. This value is obtained by means of a battery of simulations for different values of s, and the obtained U_e values are compared with those obtained from the simulation of the case without fins. For this analysis, the thickest plate (e= 5 cm) is considered, since for that case the effect of the fins is bigger. The results obtained from this battery of simulations are summarized in Fig A-1 in a dimensionless way. It can be observed that the effect of the fins becomes negligible for relations of e/s over 1.2.

Thus, for the current case the maximum value for s is set at 7.65 cm considering the encapsulation thickness.

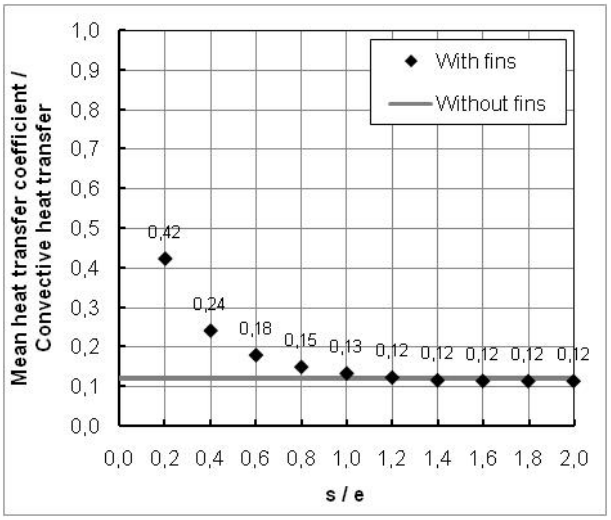

Fig. A-1. Dimensionless representation of the variation of the mean heat transfer coefficient with the fin separation

A total of 40 combinations have been selected for this purpose and the next empirical expressions have been obtained, where the values of e and x are expressed in m. Statgraphics software [21] was used to make the adjustment and it was found a very good agreement with the simulated values.

Table A- 1. General analytical expressions for the mean heat transfer coefficients

	Formula	R^2-adj	St. error (W/m^2K)
$U_{e,c}$	$\frac{-52.61+96.7\sqrt{1+11.23\frac{e}{s}}+[15.97+86.31(e-s)]^2+\left(0.068+\frac{9.8\times10^{-4}}{s^2}\right.}{\frac{4.26}{1+\ln(e^2+s)}+\frac{199.021}{1+113.23(e-s)^2}}$	99.72%	±3.77
$U_{e,d}$	$\frac{-55.45+\frac{1.752}{s(1+s)}+144.02\exp\left[-85.415\,(e+s)/\sqrt{e^2+s^2}\right]+75.14\sqrt{1+0.4}}{\frac{111.29}{1-1.76(e+s)/\sqrt{e^2+s^2}}-\frac{259.49}{1-95.38(e^2-s)}}$	99.94%	±1.87

REFERENCES

[1] Sharma A, Tyagi VV, Chen CR, Buddhi D. Review on thermal energy storage with phase change materials and applications. Renewable and Sustainable Energy Reviews 2009; 13(2): 318-345.

[2] Dutil Y, Rousse DR, Salah NB, Lassue S, Zalewski L. A review on phase change materials: Mathematical modeling and simulations. Renewable Sustainable Energy Rev 2011;15:112-30.

[3] Crank J. Free and moving boundary problems. Oxford: Clarendon Press; 1984.

[4] Hill JM. One-dimensional Stefan problems: an introduction. Harlow: Longman Scientific Technical; 1987.

[5] Carslaw HS, Jaeger JC. Conduction of heat in solids. Oxford: Clarendon Press; 1959.

[6] Humphries WR, Griggs EI. A Design Handbook for Phase Change Thermal Control and Energy Storage Devices. NASA Technical Paper 1977; 1074.

[7] Stritih U. An experimental study of enhanced heat transfer in rectangular PCM thermal store. Int J Heat Mass Tran 2004; 47:2841-7.

[8] Lamberg P, Lehtiniemi R Henell AM. Numerical and experimental investigation of melting and freezing processes in phase change material storage. Int J Therm Sci 2004; 4:277-87.

[9] Wang Y, Yang Y. Three-dimensional transient cooling simulations of a portable electronic device using PCM (phase change materials) in multi-fin heat sink. Energy 2011; 36(8): 5214-24.

[10] Colella F, Sciacovello A, Verda V. Numerical analysis of a medium scale latent energy storage unit for district heating systems. Energy 2012; 45(1): 397-406.

[11]MacPhee D, Dincer I,Beyene A. Numerical simulation and exergetic performance assessment of charging process in encapsulated ice thermal energy storage system. Energy 2012; 41(1): 491-8.

[12] Lamberg P, Siren K. Approximate analytical model for two-phase solidification problem in a finned phase-change material storage. Appl Energ 2004; 77: 131-52.

[13] Singh RD, Tiware GN. Energy conservation in the greenhouse system: A steady state analysis. Energy 2012; 35(6): 2367-73.

[14] Dolado P, Lazaro A, Marín JM, Zalba B. Characterisation of melting and solidification in a real scale PCM-air heat exchanger: Numerical model and experimental validation. Energ Convers Manage 2011; 52:1890-907.

[15] Hed G Bellander R. Mathematical modeling of PCM air heat exchanger. Energ Buildings 2006: 38:82-9.

[16] Shamsundar N, Sparrow E. Analysis of multi-dimensional conduction phase change via the enthalpy model. J Heat Transf 1975; 97: 333-40.

[17] Campos-Celador A, Urbikain K, Diarce G, Sala Lizarraga JM. Analysis of the natural convection in a plate-and-fins latent thermal energy storage system using the CFD technique. Proceedings at: INNOSTOCK 2012.The 12th International Conference on Energy Storage . 2012.

[18] Çengel YA. Heat Transfer: A practical approach. 2nd ed. Boston: McGraw-Hill; 2002.

[19] Bejan A. Two thermodynamic optima in the design of sensible heat units for energy storage. J Heat Transf 1978; 100: 708-12.

[20] European co-operation for Acreditation. EA-4/02: Expression of the Uncertainty of Measurent in Calibration. 1999.

[21] STATGRAPHICS® Centurion XVI User Manual; 2009.